Received: 8 April 2021 | Accepted: 18 July 2021

DOI: 10.1111/ppa.13451

Plant Pathology WILEY

ORIGINAL ARTICLE

Temporal and spatial propagule deposition patterns of the emerging fungal pathogen of chestnut *Gnomoniopsis castaneae* in orchards of north-western Italy

Guglielmo Lione[1,2] | Luana Giordano[1,2] | Fabiano Sillo[1,3] | Francesca Brescia[1] | Paolo Gonthier[1,2]

[1]Department of Agricultural, Forest and Food Sciences (DISAFA), University of Torino, Grugliasco, Italy

[2]Chestnut R&D Center, Chiusa di Pesio, Italy

[3]National Research Council - Institute for Sustainable Plant Protection (CNR-IPSP), Torino, Italy

Correspondence
Paolo Gonthier, Department of Agricultural, Forest and Food Sciences (DISAFA), University of Torino, Largo Paolo Braccini 2, I-10095 Grugliasco, Italy.
Email: paolo.gonthier@unito.it

Present address
Luana Giordano, Laboratory of Lombardy Plant Health Service, c/o Fondazione Minoprio, Vertemate con Minoprio, Italy

Funding information
University of Torino; Regione Piemonte; European Commission, Grant/Award Number: 540693

Abstract

Two chestnut (*Castanea sativa*) orchards of north-western Italy were sampled with passive spore traps 35 times over 24 months. Samples were analysed through a newly developed quantitative PCR assay to quantify propagule loads of the emerging fungal pathogen *Gnomoniopsis castaneae*. Average propagule deposition patterns were assessed along with temporal and climatic variables, including sampling month and season, temperatures, relative humidity, precipitations, and wind. Machine learning algorithms combining information theory, fractal analysis, unbiased recursive partitioning, ordinary least squares and logistic regressions, were used to model propagule deposition patterns. The trained models were validated on independent data gathered from 24 samplings conducted in a third chestnut orchard during the same timeframe. Results showed that propagule deposition rate (DR) was variable within and among sites, with a site average ranging from 173 to 765 spores $\cdot m^{-2} \cdot h^{-1}$. Propagule deposition was observed across all seasons, although the DR dropped substantially during wintertime ($p < 0.05$). Mean, maximum, and minimum temperatures, the growing degree days at 0 and 5°C thresholds, and wind gust were all positively correlated ($p < 0.05$) with DR of *G. castaneae*. The trained models were all significant ($p < 0.05$), as well as their validation ($p < 0.05$). Fluctuations of propagule deposition throughout the year were consistent among sites and proved to be driven by temperatures. Wind gust was associated with the overall amount of propagules deposited at site level. In future, the increase in temperatures and strong winds as a result of climate change may boost the spread of *G. castaneae*.

KEYWORDS
aerobiology, *Castanea*, climate, epidemiology, *Gnomoniopsis smithogilvyi*, nut rot

1 | INTRODUCTION

Aerobiology is a field of research dating back to the early 1700s and its application to plant pathology has become increasingly important over the centuries. Fungal and fungal-like plant pathogens may release viable airborne propagules, that is, sexual spores, asexual conidia, or sporangia, potentially able to infect susceptible hosts through active or passive penetration, thereby spreading diseases at short, medium, or long distance depending on the pathogen species and environmental conditions (Kendrick, 2017). Indeed, airborne inoculum plays a key epidemiological role by increasing the distribution range of plant pathogens at the local, regional, and continental scales, as extensively documented in the literature (Viljanen-Rollinson et al., 2007, and references therein). For instance, since its introduction to England in 1845, the North American grape pathogen *Erysiphe necator* invaded the whole Mediterranean basin in no longer than 7 years (Kendrick, 2017). More recently, the causal agent of ash dieback *Hymenoscyphus fraxineus* has invaded most of its host distribution range since it was introduced to Europe from Asia in the 1990s (Kowalski, 2006). Epidemics on both grapes and ashes occurred as a result of dispersal of pathogen airborne inoculum (Kendrick, 2017), but these are only two examples among numerous others.

The quantification of infectious spore loads of plant pathogens through properly designed aerobiological assays may be pivotal to implementing effective surveillance networks and early warning systems for plant protection and biosecurity enhancement (Thomas et al., 2017). In addition, unravelling the temporal or spatial propagule deposition patterns of target plant pathogens may shed light on their biology, ecology, and epidemiology. A better understanding of such aspects can lead to better plant disease management (Garbelotto et al., 2017; Gonthier et al., 2005; Thomas et al., 2017). Although different aerobiological assays are available (reviewed in Jackson & Bayliss, 2011; West & Kimber, 2015), they all rely on spore trapping devices collecting airborne propagules, and on diagnostic methods detecting and quantifying propagules of target pathogens. Spore trapping devices are defined as passive when the spore loads suspended in the air spontaneously deposit upon an appropriate surface by gravitation and include, for example, Petri dishes, filter papers, wood discs, buckets and rain samplers. Conversely, active spore traps have mechanisms for the assisted interception of the spores floating in the air, such as vacuum pumps in Hirst and Burkard devices, and moving components in rotating arm or similar impactors. Once the sample has been collected, the airborne inoculum of the target pathogen can be detected and possibly quantified by means of optical or electron microscopy, PCR- or loop-mediated isothermal amplification (LAMP)-based assays, or with immunoassays. Each of these methods has its own pros and cons depending on the target species, the desired precision of spore quantification, field and laboratory technical constraints, the level of expertise required to carry out the entire analyses, and the cost.

Thus, assessing temporal or spatial propagule deposition patterns is important to implement surveillance programmes and undertake timely actions for disease control; however, the identification of which factors, either temporal and/or environmental, may explain the observed patterns can also be useful. Not surprisingly, several studies have attempted to investigate and quantify the role played by such factors in the sporulation of fungal or fungal-like pathogens. Such investigations have been carried out for *Alternaria* spp. (Skjøth et al., 2016), *Chrysomyxa rhododendri* (Ganthaler & Mayr, 2015), *E. necator* (Willocquet & Clerjeau, 1998), *Gremmeniella abietina* (Petäistö & Heinonen, 2003), *H. fraxineus* (Grosdidier et al., 2018), *Lecanosticta acicola* (Wyka et al., 2018), *Heterobasidion* spp. (Gonthier et al., 2005), *Phytophthora ramorum* (Garbelotto et al., 2017), among many others reported in the literature. The understanding of factors associated with propagule deposition patterns of plant pathogens is often a prerequisite for moving further and modelling such patterns based on temporal or environmental variables (Garbelotto et al., 2017; Gonthier et al., 2005; Van Maanen & Xu, 2003). The rationale of this modelling approach relies on the evidence that temporal (e.g., daytime, weeks, months, seasons, years) and environmental variables, especially climatic ones (e.g., temperatures, precipitations, relative humidity, wind speed) are usually associated with the production, liberation, and dispersal of airborne inoculum (Garbelotto et al., 2017; Gonthier et al., 2005; Kendrick, 2017; Lovell et al., 2004). For instance, temperatures are major drivers of processes leading to sporulation, and some studies have even suggested the replacement of seasonal and temporal variables with temperature-related variables, such as the growing degree days or "thermal time" (Lovell et al., 2004). Temperature and temperature accumulation have been reported as highly correlated with several ontogenic phases of plant pathogens, encompassing sporulation, spore maturation, and spore release, and they are also closely related to disease incidence (Gonthier et al., 2005; Lione et al., 2015; Lovell et al., 2004). Relative humidity and precipitation are other key explanatory variables of propagule production, discharge, and transportation in fungi (Hasnain, 1993). Wind is expected to play a major role in the dispersal of the airborne inoculum not only as passive carrier of propagules, but also as factor triggering the liberation of inoculum (Kendrick, 2017). Temporal and environmental variables are not only associated with the production, liberation, and dispersal of airborne inoculum of plant pathogens, but they are also widely available, accessible or easy to measure (Lovell et al., 2004). Such variables have proved to be particularly suitable for testing hypotheses, and predicting the effects and trends of epidemics, as well as to conceptualize complex host–pathogen–environment interactions (Van Maanen & Xu, 2003).

The ascomycete pathogen *Gnomoniopsis castaneae* (Visentin et al., 2012), also referred to as *G. smithogilvyi* (Shuttleworth et al., 2012), is recognized as one the most serious emerging threats to chestnut (*Castanea* spp.) cultivation worldwide, mainly because of the losses it is causing in Europe and Australasia as a nut rot agent (Lione et al., 2019). However, the fungus has also been reported in association with cankers on twigs, scions, and branches and as an endophyte in green tissues of chestnut (Lione et al., 2019; Pasche et al., 2016; Visentin et al., 2012). The fungus is characterized by having both a teleomorphic stage, producing perithecia on burrs,

and an anamorphic stage, producing acervuli on galls of the Asian gall wasp *Dryocosmus kuriphilus* and on cankers (Lione et al., 2019; Pasche et al., 2016; Visentin et al., 2012). Floral infection by means of ascospores or conidia leads to the onset of nut rot (Shuttleworth & Guest, 2017; Visentin et al., 2012), although other infection pathways cannot be ruled out (Lione et al., 2019). While both ascospores and conidia are infectious, there is still little information available about airborne inoculum potential and propagule deposition patterns of the fungus in time and space, as well as on the role of temporal and climatic variables on such patterns.

Therefore, the goals of this study were (a) to assess the temporal and spatial propagule deposition patterns of *G. castaneae* in orchards of north-western Italy using a passive spore trapping method, (b) to test which temporal and climatic variables are associated with such deposition patterns, and (c) to model these propagule deposition patterns accordingly. A taxon-specific quantitative PCR (qPCR) assay for the identification and quantification of *G. castaneae* propagules captured by the passive spore traps was also developed and tested.

2 | MATERIALS AND METHODS

2.1 | Study sites, experimental design, and samplings

Based on the distribution of *G. castaneae* previously assessed in north-western Italy (Lione et al., 2015; Visentin et al., 2012), three study sites were selected in the municipalities of San Giorio di Susa (training site 1—TS1), Peveragno (training site 2—TS2) and Gaiola (evaluation site—ES). The main characteristics of the study sites are reported in Table 1. All study sites were covered by chestnut orchards across the entire surface, accounting for approximately 4 ha per site, and they were mostly surrounded by other chestnut orchards and coppices. The mean diameter of trees at breast height ranged from 46 cm in ES (*SD* = 10 cm) to 56 cm in TS2 (*SD* = 13 cm) and 67 cm in TS1 (*SD* = 16 cm).

A linear transect of 130 m was tracked within each site (Figure S1), consisting of 14 spore trap devices placed at a regular distance of 10 m from one another. Based on the method described in Garbelotto et al. (2008), a passive spore trap device was built using a 150-mm-diameter disc of Whatman filter paper sterilized at 121°C for 20 min, fixed on a sterile plastic Petri plate with a diameter of 15 cm by a 0.5 mm-thick sterile copper cable. Under a biological hood, the cable was passed through two 0.7 mm holes drilled along the diameter of both the paper disc and the Petri plate, at 3 cm from the centre. Subsequently the paper was dampened with 20 ml 4× TE buffer solution (40 mM Tris.HCl at pH 8.0, 4 mM EDTA) to prevent DNA degradation as well as spore germination (Garbelotto et al., 2008; Grosdidier et al., 2017). Spore trap devices were supported by a tripod made with 1 cm-diameter plastic sticks with a length of 2 m. The tripod was anchored in the ground to a depth of 30 cm, allowing the spore device to be exposed horizontally at a height of approximately 1.50 m, which was largely over the mean height of the understorey. Exposure to the air in this way allowed for gravitational deposition of the airborne inoculum of *G. castaneae* onto the filter papers. The tripod and the spore trap device were stabilized and reinforced with tightened copper (0.5 mm diameter) and iron cables (1 mm diameter). Once mounted and placed along the linear transect, the tripods were labelled progressively from 1 to 14 and left in the same position for 2 years, from 15 October 2013 to 27 October 2015 (Figure S2). Depending on technical and meteorological constraints limiting the accessibility of sites, TS1 and TS2 were sampled on the same days at intervals ranging from a minimum of 12 to a maximum of 41 days, with an average of 21 days. Overall, 35 samplings were conducted in TS sites over the 2 years. The same design was used in ES, but in this case, a subset of 24 samplings was conducted and split in order to include an approximately equal number of samplings for each season. Samplings in ES were synchronized with those conducted in TS sites to allow for data comparison among sites. At every sampling, each spore trap device was removed and replaced with a new sterile one, with buffer-dampened filter paper, as described above. The filter papers were sheltered from the sun by the chestnut canopy, protecting them from drying and possibly preventing DNA degradation. After removal, the exposed filter paper was stored in a 50 ml Falcon tube, labelled with the corresponding tripod number, and transported to the laboratory where it was stored at −80°C prior to DNA extraction.

To confirm the presence of the fungus in the study sites, the incidence of *G. castaneae* (%) was assessed at nut harvesting time (September–October) from 2013 to 2015, by randomly collecting a sample of 40 nuts from each study site. Sample collection, fungal isolation, and identification of *G. castaneae* were conducted as described in Lione et al. (2015).

2.2 | Primer design for the development of a taxon-specific qPCR assay for *G. castaneae*

A taxon-specific qPCR primer set targeting *G. castaneae* was designed using the internal transcribed spacer (ITS) alignment previously employed by Lione et al. (2015) to design an end point PCR primer set for the pathogen. The published sequences of the ITS region of *G. castaneae* (Sillo et al., 2017; Visentin et al., 2012) were aligned with the ITS sequences of phylogenetically closely related species available in GenBank (www.ncbi.nlm.nih.gov/genbank/). GenBank accession numbers of sequences of *G. castaneae* used were HM142946.1, HM142947.1, HM142948.1, HM142950.1, HM142955.1, HM142956.1, HM142958.1, HM142959.1, HM142960.1, LN999963, LN999964, LN999965 and LN999966. Nontarget species included in the alignment were *Apiognomonia errabunda*. (DQ313541.1), *A. veneta* (DQ994611.1), *Gnomoniopsis alderdunensis* (GU320825.1), *G. chamaemori* (GU320817.1), *G. clavulata* (EU254818.1), *G. comari* (EU254822.1), *G. fructicola* (GU320816.1), *G. idaeicola* (KC145891.1), *G. macounii* (EU254762.1), *G. occulta* (GU320828.1), *G. paraclavulata* (GU320830.1), *G.*

TABLE 1 Main characteristics of the study sites

Study site	San Giorio di Susa (TS1)	Peveragno (TS2)	Gaiola (ES)
Latitude (°)	45.1196	44.3261	44.3358
Longitude (°)	7.1852	7.5862	7.3914
Elevation (m a.s.l.)	540	605	823
Aspect	N-NE	NE	S-NE
Geographic position	Valle di Susa	Pianura Padana	Valle Stura di Demonte
Soil type	Dystric Luvisol	Eutric Leptosol	Eutric Cambisol
Hillslope	BS	FS-BS-TS	BS
Average mean temperature (°C)	10.8	12.0	10.7
Total precipitation (mm)	796	775	836
Mean diameter at breast height (cm)	67	56	46
Orchard maturity stage	Old-grown	Mature/old-grown	Mature
Tree density (trees/ha)	107	75	76
Transect minimum and maximum elevation (m)	531–548	596–614	822–824
Transect slope (%)	13	14	2
Transect orientation (°)	104	351	50

Note: Each study site is identified with the name of the municipality, along with its acronym (training sites—TS; evaluation site—ES). For each site, latitude (Lat) and longitude (Long) are provided in decimal degrees based on ellipsoid WGS1984. Aspect is indicated based on the wind rose orientation. Geographic position is provided according to the local toponyms reported in the Regional Technical Map of the Piedmont Region (Regione Piemonte - A1613B - Sistema informativo territoriale e ambientale, 2005). Soil type is gathered from the ecopedological map of Italy provided as Web Map Service (WMS) in the online National Geoportal [http://www.pcn.minambiente.it/] of the Italian Ministry for Environment, Land and Sea Protection. The hillslope position classification indicates slope morphology as backslope (BS), footslope (FS), or toeslope (TS). Average mean temperature and the total precipitation refer to the period 1970–2000, and they are derived from the 30 s precision monthly raster of the WorldClim version 2.1 (Fick & Hijmans, 2017). Mean diameter at breast height was assessed in the field along with the orchard maturity stage, which was scored based on the visual examination of the chestnut growing in each study site. Tree density refers to the number of chestnut trees per ha in the study sites. The transect minimum and maximum elevation is the elevation range included between the lower and upper bounds of the linear transect. Transect elevation and slope were obtained from the Digital Terrain Model of Piedmont Region (Regione Piemonte - DB0800 - Programmazione strategica, Politiche territoriali ed Edilizia - DB0816 - Cartografia e Sistema Informativo Territoriale, 2009), while orientation (azimuth in °) was derived from the Azimut Measurement Plugin for QGis v. 3.4.7-Madeira.

racemula (EU254841.1), *G. sanguisorbae* (GU320818.1), *G. tormentillae* (EU254856.1) and *Ophiognomonia leptostyla* (EU254910.1). Sequence alignments were performed using the ClustalW algorithm of the MEGA 5 software to detect regions conserved within *G. castaneae* isolates and displaying differences from the nontarget species, which were used to design forward and reverse primers. Primers were designed with PRIMER 3 software to achieve a Tm of at least 60°C and an amplicon size of <250 bp. The online software tool PrimerBLAST was used to perform a nucleotide BLAST analysis to determine whether the taxon-specific primers designed displayed any significant identity with sequences derived from other nontarget organisms. Designed forward and reverse primers were named Gc_SpecF, and Gc_SpecR.

2.3 | Analytical specificity of qPCR assay

In order to assess amplification specificity of the newly developed primer set, DNA samples from 25 fungal species (nontarget) and from *G. castaneae* (target) were used as template for a qPCR with the primer set designed in this study. The nontarget fungal species were isolated from chestnut nuts, lesions, burrs and from air sampled in chestnut stands (Table S1). Although no other *Gnomoniopsis* species were reported at the study sites, we included *G. idaeicola* (isolate MUT 5786) in the list of nontarget fungi, because it is the European fungal species most closely related to *G. castaneae* based on the phylogenetic analysis reported by Jiang and Tian (2019).

Prior to DNA extraction, isolates were grown in 2% malt extract broth at 25°C for 1 week. Freeze-dried mycelium (approximately 200 mg) for each isolate was homogenized in liquid nitrogen and disrupted using two glass beads (0.2 mm diameter) in a FastPrep Cell Disrupter (FP220-Qbiogene). DNA extraction from mycelia was performed using an EZNA Stool DNA Kit (Omega Bio-Tek).

The qPCR was carried out with a Connect Real-Time PCR Detection System (Bio-Rad Laboratories). Each qPCR was conducted in a total volume of 10 μl, containing 1 μl DNA, 5 μl SsoAdvanced Universal SYBR Green Supermix (Bio-Rad Laboratories), 0.2 μl of each primer (3 μM) and 3.6 μl of water, using a 96-well plate. A negative control (water) was also included in each plate, as well as two positive controls represented by two isolates of *G. castaneae* from two different subpopulations found in Italy (isolate PV31 for subpopulation 1 and MTT8 from subpopulation 2; Sillo et al., 2017). For each sample, including negative and positive controls, two technical replicates were used. The following PCR protocol was adopted: 98°C for 2 min; 40 cycles of 98°C for 5 s, 61°C for 10 s. Fluorescence data points were acquired at the end of the extension step and amplification threshold cycle (C_t) values of samples and controls were obtained directly from the instrument. Melt curve analysis was also performed and parameters were as follows: ramp from 65 to 95°C with a temperature increment of 0.2°C and a read every 5 s.

Primer specificity for *G. castaneae* was tested against *G. idaeicola* with the qPCR assay and melt curve analysis described above, but, in addition, a high-resolution melt curve analysis (HRM) was also conducted using the Precision Melt Analysis software v. 4.0.52.0602 (Bio-Rad). Moreover, electrophoresis on a 1% agarose 1% MetaPhor (Lonza Bioscience) gel (wt/vol) was performed for 100 min at 4 V/cm to ensure an accurate fragment separation. The gel was then stained with GelRed (1 μg/ml; Biotium) and visualized on a GelDoc EZ Imager (Bio-Rad).

2.4 | Analytical sensitivity of qPCR assay

In order to determine the limit of detection (LOD) and quantification (LOQ) of the newly developed primer set, the DNA extracts from two isolates of *G. castaneae* (MTT8 and PV31) were serially diluted five times (from 0.03 ng/μl to 3 fg/μl) into two different diluting media. Milli-Q sterile water was used to dilute the DNA for determining the LOD in the absence of nontarget DNA (water medium), whilst DNA extracts from a spore trap exposed in chestnut orchards and negative to *G. castaneae* DNA in a qPCR assay was used to test whether the presence of nontarget DNA was affecting the LOD (environmental medium). For each dilution, six technical replicates were used. Two negative controls were included, one for the water and one for the environmental medium, with two technical replicates each. The qPCRs were carried out as described for the specificity assay. For each medium, a standard curve was generated. The LOD and LOQ were calculated according to Desimoni and Brunetti (2015) as LOD = 3.3*SD*/s and LOQ = 10*SD*/s, where *SD* is the standard deviation of the *y* intercept and s is the slope of the curve.

In order to determine LOD and LOQ on DNA extracts from spore traps and to generate a standard curve to be used in quantitative analysis of airborne inoculum, 18 spore trap devices (three sets of six spore traps each) were prepared in the laboratory as described above and sprayed with 1 ml of conidial suspension of *G. castaneae*. The suspension of *G. castaneae* conidia was prepared from liquid culture of *G. castaneae* isolate BOF25 (Sillo et al., 2017) grown in 2% malt extract broth at 25°C for 7 days in the dark with agitation. Conidia were collected, counted in a Bürker chamber using an optical microscope, and their concentration was adjusted to 10^6 conidia/ml by adding sterile water. The suspension was subsequently serially diluted from 10^6 conidia/ml to 10 conidia/ml and used to spike six clean paper discs. Each set of spore devices was wetted with one of the following serial concentrations of conidial suspension: 10^1, 10^2, 10^3, 10^4, 10^5, and 10^6 conidia/ml.

Subsequently, total DNA was extracted from the paper discs using a CTAB-based protocol. Paper discs were cut into slices (approximately 10 mm in width) by using sterilized scissors, placed in 50 ml Falcon tubes filled with 20 ml of warmed (65°C) TE buffer, vortexed for 5 min, and centrifuged at 875 × *g* for 60 min. Subsequently, paper slices were removed and the remaining solution vortexed again (5 min) and centrifuged at 875 × *g* for 5 min. The supernatant was carefully removed and the pellet containing spores/conidia was resuspended in 100 μl of sterile water and transferred in 2 ml Eppendorf tubes. Samples were then homogenized with Glass Beads X (EZNA Stool DNA Kit) in the FastPrep Cell Disrupter, for 30 s at 5 Hz. Homogenized samples were resuspended in 300 μl of a CTAB extraction buffer (100 mM Tris-HCl pH 8.4, 1.4 M NaCl, 25 mM EDTA pH 8.0, 2% CTAB), vortexed, frozen in liquid nitrogen for 2 min and incubated at 65°C for 2 min. This step was repeated twice, and an additional incubation at 65°C for 3 min was carried out at the end. After extraction, an equal volume of chloroform/isoamyl alcohol (24:1) was added to each tube, and tubes were vortexed, and then centrifuged for 10 min at 12,300 × *g* in a microcentrifuge. The upper phase was transferred to a 1.5 ml Eppendorf microcentrifuge tube where the DNA was precipitated by the addition of 600 μl of cold isopropanol and centrifugation at 15,366 × *g* for 5 min. Subsequently, the supernatant was discarded and the DNA pellet was gently washed with 70% ethanol and resuspended in 30 μl TE buffer by heating at 65°C for about 30 min. Extracted DNA was used in qPCR as described above and a standard curve for serial dilutions of conidia extracted from spore traps was generated. In addition, the LOD and LOQ were calculated.

2.5 | Quantification of *G. castaneae* airborne propagules by qPCR

A qPCR assay was set up to quantify the airborne inoculum of the pathogen using the newly designed primers Gc_SpecF and Gc_SpecR and the total DNA extracted from the spore trap devices sprayed with the suspensions of *G. castaneae* conidia at known concentration as described in the previous sections. Starting

concentrations of DNA and number of spores/conidia deposited onto spore traps in the field were determined by analysing the C_t of samples and comparing them to the standard curve. The qPCR efficiency (E) was calculated from the slope (s) of the line using the equation $E = 10^{\frac{-1}{s}} - 1$. The qPCR results were considered acceptable for analysis if the standard curve slope was between 2.9 and 3.5, the R^2 was above 0.97, and efficiency values of the plate were between 0.90 and 1.10.

The qPCR assay was performed with a Connect Real-Time PCR Detection System (Bio-Rad Laboratories). Each qPCR was conducted in a total volume of 10 μl, containing 1 μl DNA of samples, 5 μl SsoAdvanced Universal SYBR Green Supermix (Bio-Rad Laboratories), 0.2 μl of each primer (3 μM) and 3.6 μl of water. A negative control (water) was also included in each plate, as well as two positive controls (*G. castaneae* DNA). For each sample two technical replicates were used, and the following PCR protocol was adopted: 98°C for 2 min; 40 cycles of 98°C for 5 s, 61°C for 10 s. Fluorescence data points were acquired at the end of the extension step and C_t values of samples and controls were directly obtained from the instrument. Melt curve analysis was also performed and parameters were as follows: ramp from 65 to 95°C with a temperature increment of 0.2°C and a read every 5 s. Melt curves were analysed using the Bio-Rad CFX Manager software. To exclude the presence of *G. idaeicola* in the samples of DNA extracted from the spore traps, a subset of 19 samples from all study sites was randomly selected among those positive to the qPCR assay (Table S2). The 19 samples were processed with the same qPCR assay including the isolates of *G. castaneae* MTT8 and *G. idaeicola* MUT 5786 as positive controls. A negative control (water) was also included and two technical replicates of each condition were used. Melt curves were analysed by using the Bio-Rad CFX Manager software and the Precision Melt Analysis software. Subsequently, an electrophoresis was carried out as described above.

In order to confirm that absence of amplification truly indicated absence of *G. castaneae* DNA, samples that did not amplify were subjected to PCR with the universal eukaryotic primer set (ITS1/ITS4; White et al., 1990). The PCR mix included 6.25 μl of DNA, 0.025 U *Taq* DNA polymerase (Promega), 0.5 μM of each primer, 200 μM of each dNTP (deoxynucleotide triphosphate), and 5 μl of the 5× buffer in a total volume of 25 μl. The PCR protocol comprised a denaturation step at 94°C for 3 min; followed by 35 cycles of 94°C for 30 s, 54°C for 30 s, and 72°C for 45 s; and a final elongation step at 72°C for 10 min. Negative (water) and positive (*G. castaneae* DNA of isolate BOF25; Sillo et al., 2017) controls were included in the reactions. The PCR amplicons were visualized using GelRed (1 μg/ml; Biotium) on 1% (wt/vol) agarose gel after electrophoresis at 6 V/cm for 30 min.

Because the diameter (see above) and surface of paper discs used in the DNA extraction was known, it was possible to assess the number of spores/conidia on the surface of discs (in cm^2) from their concentration per μl (determined by intersection of C_t of samples with the standard curve). This value was normalized for the number of hours that spore traps were exposed to obtain the deposition rate (DR) of the airborne inoculum of *G. castaneae* expressed as spores $\cdot m^{-2} \cdot h^{-1}$ (File S1).

2.6 | Collection of temporal and climatic data

Both temporal and climatic variables associated with the sampling time or the study sites were collected. The month of each sampling date (ms) and the corresponding meteorological season (sm) were recorded as temporal variables. The variable sm included December, January, and February in winter; March, April, and May in spring; June, July, and August in summer; and September, October, and November in autumn.

A weather station was placed at all sampling sites, with temperature (°C), relative humidity (%), and rainfall (mm) sensors and equipped with a data logger (Onset Hobo series). Data for other climatic variables, not measurable with the available equipment, were retrieved from the nearest official meteorological stations of the Meteorologic and Hydrologic Database of the Regional Agency for Environmental Protection of Piedmont (ARPA Piemonte, 2020). For TS1, TS2, and ES, meteorological ARPA stations no. 143 (lat. 45.11642°, long. 7.24393°), no. 575 (lat. 44.33510°, long. 7.56199°), and no. 765 (lat. 44.31633°, long. 7.31215°) were used, respectively. Overall, 21 climatic variables were gathered on a daily basis during the whole course of the experiment, including mean, maximum, and minimum temperatures (t_{mean}, t_{max}, t_{min}, °C); the growing degree days (°C) with threshold 0°C (gdd0), or 5°C (gdd5); the precipitation (p, mm); the number of days with precipitations exceeding the thresholds of 0, 1, 2, 5, 10, 15, 20, 25, and 30 mm (ndp0, ndp1, ndp2, ndp5, ndp10, ndp15, ndp20, ndp25, and ndp30, respectively); the mean, maximum, and minimum relative humidity (rh_{mean}, rh_{max}, rh_{min}, %); the wind speed (ws, m/s), wind gust (i.e., the maximum wind speed measured during the 24 h, wg, m/s), and timeframe of calm wind (i.e., the number of minutes during the 24 h with wind speed lower than 0.3 m/s, tcw). Wind direction was discarded because the amount of missing data was considered excessively high.

2.7 | Data preparation

The machine learning approach used in this study was deployed following the steps reported in Lantz (2019): data collection, data preparation, model training, and evaluation. Data collection was mostly covered by the operations described in the sections above.

In the data preparation step, the DR (in spores $\cdot m^{-2} \cdot h^{-1}$) of *G. castaneae* within sampling dates was averaged among spore trap devices for the three study sites separately. Mean values were calculated along with their associated 95% bias-corrected and accelerated confidence intervals with 10^4 bootstrap resamplings, hereafter referred to as $CI_{95\%}$. Temporal propagule deposition patterns of *G. castaneae* were visualized as a chronological series of the average DR values assessed during the 2 years of the experiment at each site. The series was transformed by ranking and

rescaling the average DR within a range bounded between 0 to 1 (Wickham, 2010). The transformed value was defined as standardized deposition rate (SDR). The fractal dimension (D) of the DR and SDR series was appraised with the madogram estimator to assess the variability and irregularity of the temporal spore deposition pattern of *G. castaneae* in TS1 and TS2 (Gneiting et al., 2012). The DR patterns of ES was excluded from the calculation of D because of the missing samplings. The values attained by D were compared to the bounds of its theoretical variation range, which was between 1 (i.e., low fluctuations and mild variability of the series) and 2 (highly fragmented and irregular pattern) as described in Gneiting et al. (2012). For TS1 and TS2, the site effect on DR and SDR was assessed through the unbiased recursive partitioning conditional inference tree model (Hothorn et al., 2006; subsequently referred to as ctree) that was fitted as described in Lione et al. (2020). The mutual information (MI in nats, natural units of information) shared by sites TS1 and TS2, and the coefficient of variation (CV) were calculated for both DR and SDR.

Based on the results obtained from the fractal dimension, from site effect and mutual information analyses (see Section 3), data from TS1 and TS2 were combined in the training set (TS) used to carry out the models training step. The temporal and climatic variables were referred to each sampling date within TS1, TS2, and ES using an appropriate function. For the sampling month (sm) and meteorological season (ms), the identity function was used, gathering the variables SM and MS, respectively. To derive the input climatic variables for modelling, the same method described in Garbelotto et al. (2017) was used, applying either the sum or the mean of the climatic variables in the timeframe of 7, 14, 21, and 30 days before sampling. The sum was applied to gdd0, gdd5, p, ndp0, ndp1, ndp2, ndp5, ndp10, ndp15, ndp20, ndp25, and ndp30, hence obtaining the new variables $GDD0_i$, $GDD5_i$, P_{sumi}, $NDP0_i$, $NDP1_i$, $NDP2_i$, $NDP5_i$, $NDP10_i$, $NDP15_i$, $NDP20_i$, $NDP25_i$, and $NDP30_i$, where the index i indicates the reference timeframe of 7, 14, 21, and 30 days before sampling. Similarly, the mean was applied to t_{mean}, t_{max}, t_{min}, p, rh_{mean}, rh_{max}, rh_{min}, ws, wg, tcw gathering T_{meani}, T_{maxi}, T_{mini}, P_{meani}, RH_{meani}, RH_{maxi}, RH_{mini}, WS_i, WG_i, and TCW_i. A first screening of temporal and climatic variables significantly associated with SDR was performed by applying one ctree to both SM and MS, and one ctree to each quartet (i.e., $i = [1,2,3,4]$) of climatic variables. Only variables resulting in a significant split of the ctree ($p < 0.05$) were retained for the models training step, and the corresponding threshold was used as indicator of a significant ($p < 0.05$) change in the propagule deposition potential of *G. castaneae* based on the associated climatic variable.

2.8 | Ordinary least squares regression model training

The model training step was conducted by fitting ordinary least squares (OLS) linear regression models in the form $y = mx + q$ to SDR (y) for each climatic variable (x) retained from the previous step. One model per climatic variable was fitted, with and without intercept q, including the null model. An OLS linear regression model was retained if (a) the p value of the Ramsey reset test was larger than 0.05, indicating the correct specification of the model equation as a first degree polynomial; (b) all the model coefficients displayed a p value of the associated t statistic lower than 0.05; (c) the F test of the overall model was significant ($p < 0.05$); (d) the model residuals were normally distributed based on the outcome of the Shapiro–Wilk normality test ($p > 0.05$); and (e) the OLS linear regression $y_o = m'y_p + q'$ between observed SDR values, y_o and SDR values predicted by the model, y_p showed m' and q' not significantly different from 1 ($p > 0.05$) and 0 ($p > 0.05$), respectively (Crawley, 2013; Lantz, 2019; Piñeiro et al., 2008). The regression mentioned in (e) is also known as observed versus predicted values regression or OP regression (Piñeiro et al., 2008). In case the Ramsey reset test was significant ($p < 0.05$), a function $f(x)$ was chosen based on the spatial distribution of the points in the x and y scatterplot and the regression equation was fitted as $y = mx_{trans} + q$, with $x_{trans} = f(x)$, and by applying subsequently the steps (b) to (e) as described above. The coefficient of determination (R^2), the Theil's forecast accuracy coefficient (UII) and the corrected Akaike information criterion (AICc) were calculated for all OLS linear regressions, while 95% confidence intervals, 95% prediction intervals, and the AIC weight (AIC_{cw}) were calculated only for the retained models (Crawley, 2013; Lantz, 2019). The retained models were considered the more adequate the higher they scored for the AIC_{cw} and the lower for the Theil's UII (Crawley, 2013).

2.9 | Evaluation of OLS regression models

The evaluation step was carried out on the retained OLS linear regression models (i.e., trained models), which were run with the climatic variables gathered from the study site ES. Because data from ES had not been used for model fitting, the evaluation step consisted of a process of external validation with the aim of assessing the predictive performance of the regressions trained on data from TS (see Lantz, 2019; Lione et al., 2015; Lione & Gonthier, 2016). Once the values predicted by the trained models for the ES data set were gathered, the values observed were regressed against those predicted with an OP regression (Piñeiro et al., 2008). OP regression coefficients were tested as described in (e) of the previous section, while their linearity, F significance and normal distribution of residuals were checked using the same approach illustrated in (a), (c), and (d) of the previous section. In addition, the R^2 value achieved by the OP regression and the root mean squared error of prediction (RMSEP) were calculated to score the trained models' predictive abilities (Crawley, 2013; Lione et al., 2015). Model performances were scored the highest when maximizing the R^2 of their OP regression while minimizing their RMSEP (Crawley, 2013; Lione et al., 2015; Piñeiro et al., 2008).

2.10 | Climatic modelling of the probability associated with propagule deposition levels

To unravel which climatic variable, if any, might explain the difference between the overall averages of the DR attained by TS1 and TS2, a specific analysis was carried out by combining ctree and binary logistic regression. For ctree adaptation, the outcome variable was coded as 1 for TS1 (i.e., high DR values, in the range of 512–1127 spores·m^{-2} ·h^{-1} with a confidence of 95%) and 0 for TS2 (i.e., low DR values, in the range 115–397 spores ·m^{-2} ·h^{-1} with a confidence of 95%). A total of 21 climatic variables were averaged within month and study site (TS1 and TS2): t_{mean}, t_{max}, t_{min}, gdd0, gdd5, p, ndp0, ndp1, ndp2, ndp5, ndp10, ndp15, ndp20, ndp25, ndp30, rh_{mean}, rh_{max}, rh_{min}, ws, wg, and tcw. The above averages were inserted as input for the ctree adaptation, which was set as previously described. In addition, 95% confidence intervals were calculated for the ctree output Pr(HDR) (probability of high DR values, ranging between 512 and 1127 spores·m^{-2}·h^{-1} with a confidence of 95%) with the Blaker method. Based on the ctree outcome, which indicated that the average monthly wg was the discriminating variable separating significantly ($p < 0.05$) low from high DR values of *G. castaneae* (see Section 3), a binary logistic regression (BLR) model was fitted. In BLR, the same outcome variable of ctrees was used, while monthly average wind gust (MAWG) was included as the single predictor. BLRs were assessed as described in Lione et al. (2020): in brief, β and β_0 coefficients were calculated and checked with the Wald's test, the overall model significance was verified with the likelihood ratio test comparing the BLR to the null model, the information based criteria AICc and AICcw were derived, the 95% confidence intervals of the probability associated with the outcome variable were calculated with the Heiberger–Holland algorithm, the EPV index (number of events per variable) was gathered to assess the sampling size adequacy (i.e., adequate if EPV > 0), and the area under the relative operating characteristic curve (AUC) and its associated 95% confidence intervals were calculated and contrasted with the reference value 0.5 (Crawley, 2013). No external validation was carried out on this model because of missing meteorological data in ES.

2.11 | Spatial distribution of propagule deposition

The spatial distribution of the propagule deposition of *G. castaneae* was investigated at the site scale within TS1, TS2, and ES. The DR of the pathogen during the 2-year experiment was averaged at spore trap level and the 95% CI were derived accordingly. The same analysis was conducted by averaging the DR on a seasonal basis. The randomness of the spatial distribution of the DR along the linear transect was tested with the Bartels test. The Moran's *I* index was calculated with the related *p* value to assess whether spore trap devices were surrounded by two nearest neighbouring traps displaying similar or dissimilar average DR values. The presence of clusters and spatial discontinuity of the DR was tested by fitting a ctree model to the DR using the label of the trap as ordinal input variable. The ctree and the corresponding threshold were gathered from data as described in the previous sections.

2.12 | Software for statistical analysis and modelling

Statistical analyses and modelling were conducted with R v. 3.6.0 with the following packages: binGroup, bootstrap, DescTools, fractaldim, FSA, infotheo, lawstat, lctools, lmtest, Metrics, MuMIn, partykit, pROC, scales, and strucchange. The significance threshold was set to 0.05 for all tests.

3 | RESULTS

3.1 | Analytical specificity and sensitivity of qPCR assay

Using the designed primers Gc_SpecF, 5'-GTTTATAGGG CCACCGGCCGACC-3', and Gc_SpecR, 5'-GGAACAAACGCCC TCACGGGTGC-3', no cross-amplification was observed with 25 nontarget fungal species tested. None of those showed a melt curve above the threshold line (Figure S3), confirming the reliability and specificity of the qPCR assay combined with melt curve analysis. *G. castaneae* and *G. idaeicola* were clearly distinguishable using both the HRM and the gel electrophoresis analyses (Figure S4).

The LODs in water and environmental dilution media were estimated as 7.45 and 13.67 fg, while LOQ values attained 22.57 and 41.44 fg, respectively ($R^2 = 0.90$ and $R^2 = 0.84$; Figure S3). The values of LOD and LOQ for the qPCR assay tested on DNA extracted from serial dilutions of conidial suspension in spore traps corresponded to 69 and 211 conidia. The range of detectable and quantifiable amounts of DNA extracted from conidia was between 10^2 and 10^6 conidia/ml (Figure S3). Hence, a reliable standard curve was obtained ($R^2 = 0.98$), allowing the quantification of propagule loads from 10^2 to 10^6 spores or conidia/ml on spore traps.

3.2 | Temporal propagule deposition patterns of *G. castaneae*

From 15 October 2013 to 27 October 2015, the newly designed qPCR assay allowed the processing of 1316 spore trap devices, of which 490 were from TS1, 490 from TS2 and 336 from ES. While HRM analysis conducted on the 19 samples of DNA extracted from the spore traps provided ambiguous results, gel electrophoresis of the qPCR products always displayed an amplicon size (135 bp) clearly matching that of *G. castaneae*, while no amplicons matching *G. idaeicola* (152 bp) were observed (Figure S5).

The temporal propagule deposition patterns of *G. castaneae* displayed a large variability depending on the site and sampling date. At

the site level, DR displayed an overall average of 765 spores·m^{-2}·h^{-1} (512–1,127 $CI_{95\%}$) in TS1, 205 spores·m^{-2}·h^{-1} (115–397 $CI_{95\%}$) in TS2, and 173 spores·m^{-2}·h^{-1} (88–320 $CI_{95\%}$) in ES during the 2 years of the experiment. Within sites, a variable pattern of fluctuations, flat traits and peaks was observed in the chronological series of DR (Figure 1a). The lowest average DR was 0 spores·m^{-2}·h^{-1}, detected during winter 2013/2014 and autumn 2014 in 8.6% and 12.5% of samplings conducted in TS2 and ES, respectively. The maximum DR of 3421 spores ·m^{-2} ·h^{-1} was observed in TS1 during the summer of 2014 (Figure 1a). The values attained by the fractal dimension of the DR series in TS1 ($D = 1.999$) and TS2 ($D = 1.919$) were close to 2, thus pointing to a fragmented and irregular temporal pattern of propagule deposition.

The ranking and rescaling transformation applied to obtain the SDR series (Figure 1b) allowed for maintenance of the topological properties of the temporal propagule deposition patterns of *G. castaneae* while removing the site effect on the overall average of DR. In fact, while overall averages of the DR were significantly different between TS1 and TS2 (i.e., 765 vs 205 spores ·m^{-2} ·h^{-1}, $p < 0.05$), overall averages of SDR were not (TS1: 0.500, 0.402–0.596 $CI_{95\%}$, TS2: 0.485, 0.385–0.586 $CI_{95\%}$, $p > 0.05$). The SDR of ES attained values similar to those of TS1 and TS2, with an overall average of 0.490 (0.373–0.601 $CI_{95\%}$). The transformation from DR to SDR did not substantially affect the fractal dimension of either sites, with TS1 and TS2 displaying *D* values of 1.999 and

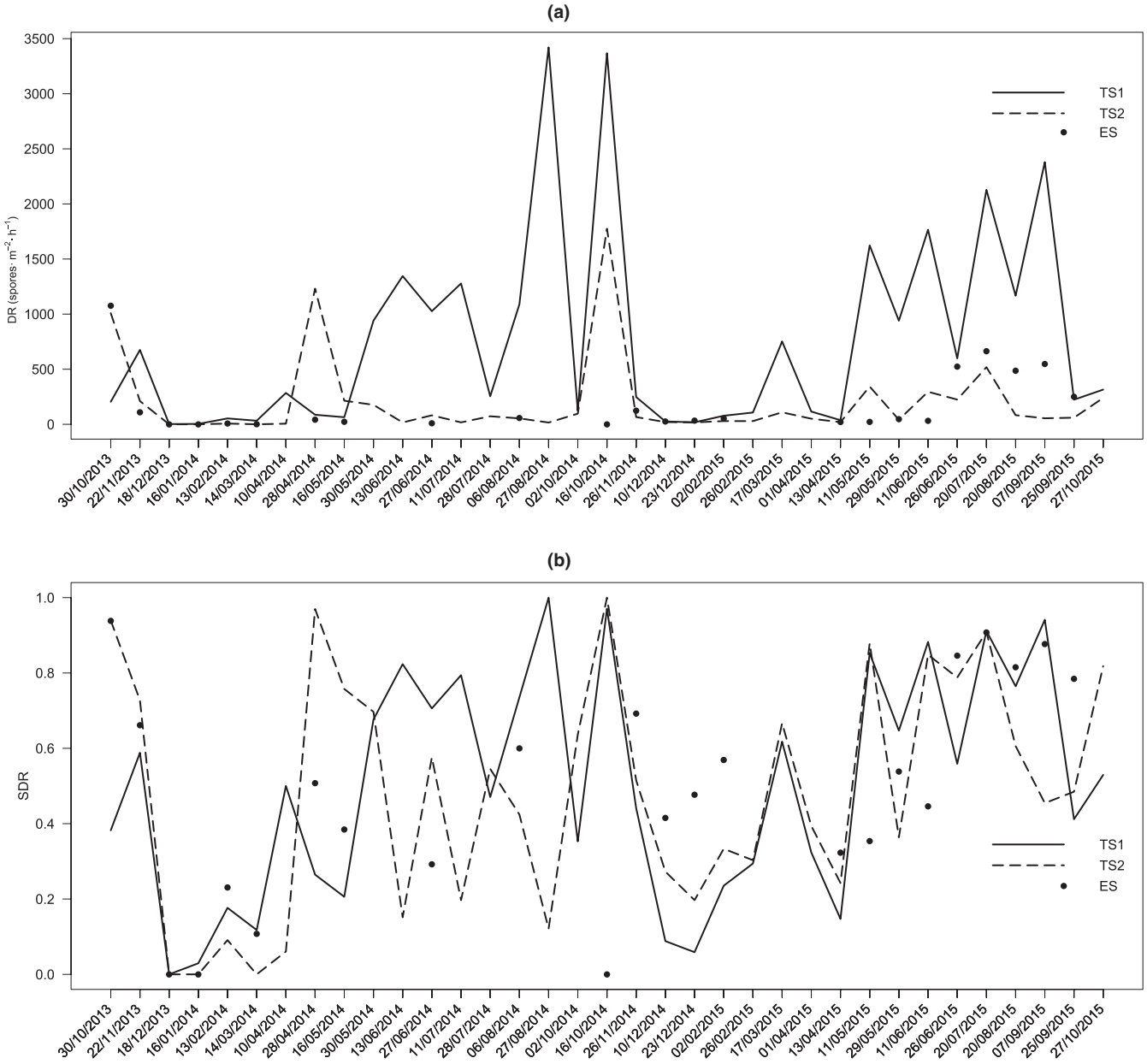

FIGURE 1 Temporal propagule deposition patterns of *Gnomoniopsis castaneae*. For each sampling date from 15 October 2013 to 27 October 2015, the average propagule deposition rate (DR) expressed as spores ·m^{-2} ·h^{-1} (a) and the standardized deposition rate (SDR) (b) are shown for the study sites TS1, TS2, and ES. Points rather than continuous lines have been used for ES. The 95% confidence intervals associated with the mean values of DR and SDR are reported in Table S3

1.824, respectively. In both cases, as observed for the DR series, *D* was close to the upper limit of its variation range indicating a highly fragmented and irregular temporal pattern of the SDR. While the coefficient of variation of DR displayed a difference of 65% between TS1 (CV = 1.211) and TS2 (CV = 1.864), this difference dropped to 4% when the coefficient of variation was calculated on the SDR, attaining CV = 0.603 in TS1 and CV = 0.640 in TS2. The presence of mutual information shared by TS1 and TS2 was detected and quantified in MI = 0.137 nats. The transformation from DR to SDR did not alter the amount of MI between TS1 and TS2.

In all three sites, the presence of *G. castaneae* was confirmed by isolations from chestnut nuts. The pathogen achieved an average incidence of 30% in TS1, 33% in TS2, and 7% in ES.

3.3 | Temporal and climatic variables associated with propagule deposition

Based on the results shown previously, data from TS1 and TS2 were combined in a single training set TS to implement the machine learning process on SDR. A total of 90 variables associated with the training set were tested, including the two temporal variables SM and MS, and the 22 climatic variables T_{meani}, T_{maxi}, T_{mini}, $GDD0_i$, $GDD5_i$, P_{sumi}, P_{meani}, $NDP0_i$, $NDP1_i$, $NDP2_i$, $NDP5_i$, $NDP10_i$, $NDP15_i$, $NDP20_i$, $NDP25_i$, $NDP30_i$, RH_{meani}, RH_{maxi}, RH_{mini}, WS_i, WG_i, and TCW_i from the four timeframes (i = [7, 14, 21, 30] days) before sampling. Hence, a total of 88 (22 × 4) climatic variables were obtained, 76 of which were derived from data collected by the meteorological sensors placed in the field in the study sites (i.e., 86% of the total number of climatic variables—T_{meani}, T_{maxi}, T_{mini}, $GDD0_i$, $GDD5_i$, P_{sumi}, P_{meani}, $NDP0_i$, $NDP1_i$, $NDP2_i$, $NDP5_i$, $NDP10_i$, $NDP15_i$, $NDP20_i$, $NDP25_i$, $NDP30_i$, RH_{meani}, RH_{maxi}, RH_{mini}, i = [7, 14, 21, 30]) and 12 from the ARPA stations (14% of the total number of climatic variables—WS_i, WG_i, and TCW_i, i = [7, 14, 21, 30]). The combined values of DR, SDR, and climatic variables of TS are provided in Table S3.

The screening process of temporal and climatic variables carried out with 23 ctrees resulted in six out of 88 variables producing significant splits ($p < 0.05$). SDR was substantially uniform during spring (0.469, 0.344–0.594 $CI_{95\%}$), summer (0.641, 0.518–0.740 $CI_{95\%}$), and autumn (0.637, 0.536–0.756 $CI_{95\%}$), but dropped significantly ($p < 0.05$) during winter (0.149, 0.09–0.212 $CI_{95\%}$; Figure 2), while no differences were detected among sampling months within seasons ($p > 0.05$).

Among climatic variables, no significant correlations were found between SDR and variables related to precipitations, number of rainy days, relative humidity, and wind ($p > 0.05$; Table S4). In contrast, the five variables T_{mean21}, T_{max30}, T_{min7}, $GDD0_{21}$, and $GDD5_{30}$ related to temperatures during the 7, 21, and 30 days before samplings displayed significant splits of ctree ($p < 0.05$), resulting in positive and significant correlations ($p < 0.05$) with the SDR. In detail, the output of ctrees revealed that the average SDR (0.629, 0.552–0.701 $CI_{95\%}$) was approximately 2.5-fold higher (significant at $p < 0.05$) above than below the T_{mean21} threshold of 10.0°C (0.260, 0.184–0.353 $CI_{95\%}$; i.e., positive correlation between SDR and T_{mean21}). Similarly, a T_{max30} over 14.6°C was associated with a significant rise ($p < 0.05$) of the SDR from 0.235 (0.161–0.320 $CI_{95\%}$) to 0.619 (0.538–0.690 $CI_{95\%}$; i.e., positive correlation between SDR and T_{max30}), and a T_{min7} exceeding 4.0°C increased the SDR significantly ($p < 0.05$) from 0.253 (0.173–0.350 $CI_{95\%}$) to 0.617 (0.537–0.689 $CI_{95\%}$; i.e., positive correlation between SDR and T_{min7}). The growing degrees days showed an effect on the SDR similar to those displayed by the mean, minimum, and maximum temperatures, with $GDD0_{21}$ and $GDD5_{30}$ significantly ($p < 0.05$) and positively correlated with higher SDR over the thresholds of 289.80°C and 154.70°C, respectively (Table S4).

3.4 | Climatic models of the temporal propagule deposition patterns

The climatic variables related to temperatures T_{mean21}, T_{max30}, T_{min7}, $GDD0_{21}$, and $GDD5_{30}$ that were significantly associated

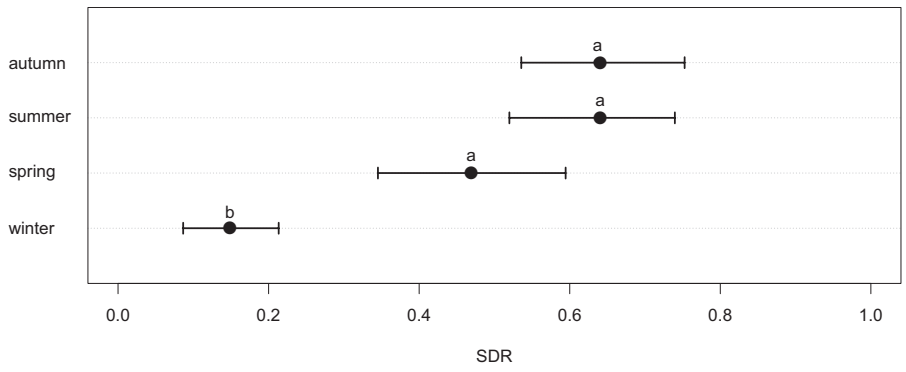

FIGURE 2 Dot chart of the average propagule deposition patterns of *Gnomoniopsis castaneae* during the four seasons. Dots refer to the average standardized deposition rate (SDR) assessed for each season during the 2-year experiment, while whiskers show the 95% bias corrected and accelerated bootstrap confidence intervals. Different letters indicate average SDR values displaying significant differences ($p < 0.05$) among seasons resulting from the corresponding unbiased recursive partitioning conditional inference tree model

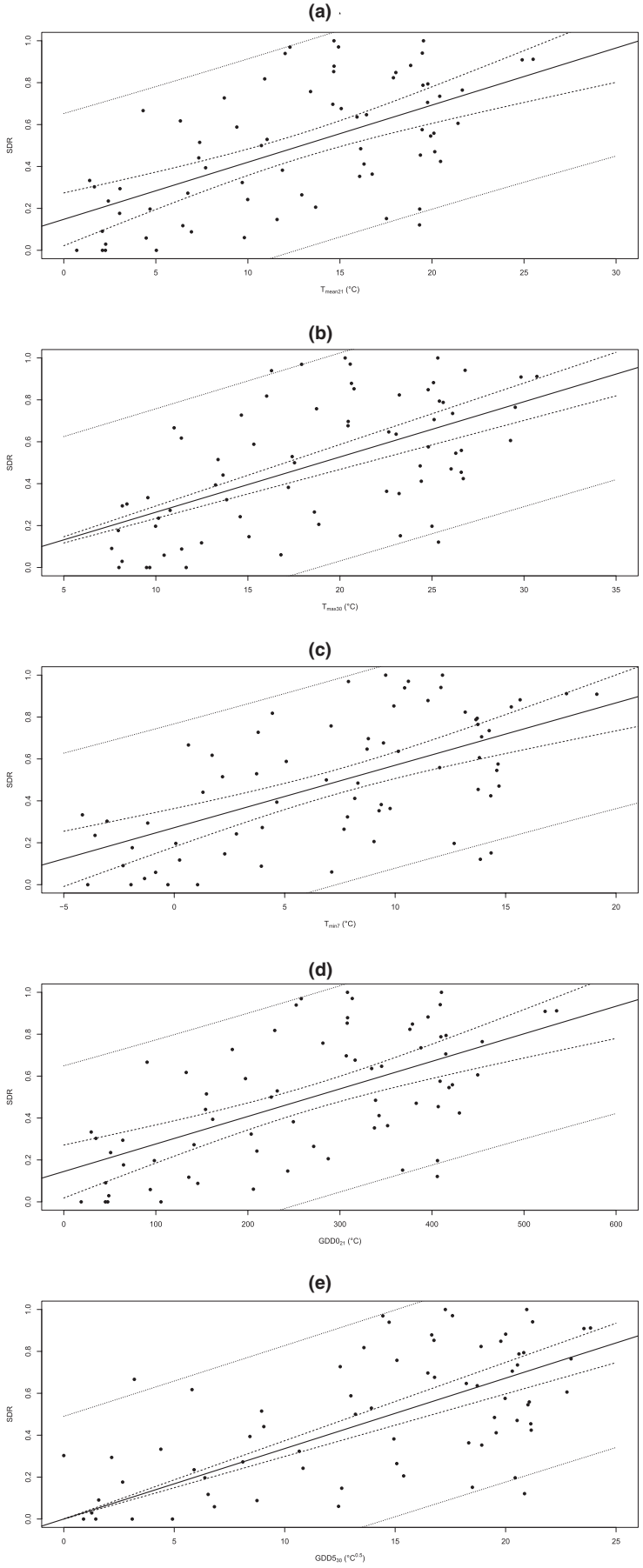

FIGURE 3 Climatic models of the propagule deposition patterns of *Gnomoniopsis castaneae* based on temperatures. Significant ($p < 0.05$) ordinary least squares linear regressions fulfilling the selection criteria in the model training step phase are presented. These models show the correlation between the standardized deposition rate (SDR, on the *y* axis) of *G. castaneae* and the following climatic variables (on the *x* axis): (a) T_{mean21} (average mean temperature of the 21 days before sampling, °C); (b) T_{max30} (average maximum temperature of the 30 days before sampling, °C); (c) T_{min7} (average minimum temperature of the 7 days before sampling, °C); (d) $GDD0_{21}$ (sum of the growing degree days with threshold 0°C of the 21 days before sampling, °C); and (e) $GDD5_{30}$ (squared root of the sum of the growing degree days with threshold 5°C of the 30 days before sampling, °C$^{0.5}$). The points indicate the observed SDR of *G. castaneae* in the training set TS, while the continuous line represents the equation of the regression model. Dashed lines show the boundaries of the 95% confidence interval of the regression, while dotted lines are the contours of the corresponding 95% prediction interval

TABLE 2 Evaluation step of ordinary least squares (OLS) linear regression models

Variable	f(x)	RT		m′		q′		FT		SWT			
		Test	p	Slope	p	Intercept	p	Test	p	Test	p	R^2	RMSEP
T_{mean21}	–	0.785	0.470	0.837	0.548	0.120	0.362	9.824	0.005	0.984	0.958	0.309	0.245
T_{max30}	–	2.158	0.141	0.907	0.744	0.080	0.566	10.370	0.004	0.984	0.954	0.320	0.240
T_{min7}	–	9.790	0.091	0.763	0.040	0.166	0.206	7.743	0.011	0.958	0.391	0.260	0.259
$GDD0_{21}$	–	0.904	0.421	0.841	0.562	0.115	0.387	9.754	0.005	0.984	0.958	0.307	0.245
$GDD5_{30}$	$\sqrt{x}$	3.420	0.053	0.712	0.160	0.196	0.525	12.900	0.002	0.970	0.671	0.370	0.250

Note: The OLS regressions fitted on the training set TS were validated with data gathered from the evaluation site ES by regressing the observed versus predicted (OP) values through OLS linear regressions.

T_{mean21} (average mean temperature of the 21 days before sampling, °C); T_{max30} (average maximum temperature of the 30 days before sampling, °C); T_{min7} (average minimum temperature of the 7 days before sampling, °C); $GDD0_{21}$ (sum of the growing degree days with threshold 0°C of the 21 days before sampling, °C); and $GDD5_{30}$ (sum of the growing degree days with threshold 5°C of the 30 days before sampling, °C).

The function used to transform x is reported, if required by the model selection procedure under the column heading f(x).

RT, FT, and SWT indicate the Ramsey reset test, the *F* test, and the Shapiro–Wilk test used to assess the OP regression linearity, significance, and the normality of the residuals, respectively. The OP regression slope (m') and intercept (q') are specified with the related *p* value resulting from the contrast against the expected values 1 and 0, respectively. The coefficient of determination (R^2) and the root mean squared error of prediction (RMSEP) are reported in association with the corresponding OP regression.

with the SDR of *G. castaneae* (Table S4) were used as predictors in the model training step. A total of 13 OLS linear regression models were fitted (Table S5), including the null model, but only five of them (Figure 3) fulfilled the conditions required for their retention. One significant model ($p < 0.05$) per climatic variable was retained as a trained model, and only in the case of $GDD5_{30}$ was the function $x_{trans} = \sqrt{x}$ applied to linearize the relation between the climatic variable and the SDR of *G. castaneae*. All trained models were concordant in showing that increasing values of T_{mean21}, T_{max30}, T_{min7}, $GDD0_{21}$, and $GDD5_{30}$ were positively and significantly correlated ($m > 0$, $p < 0.05$) with SDR. The R^2 of the OLS linear regressions ranged from a minimum of 0.358 for T_{mean21} to a maximum of 0.822 in the case of $GDD5_{30}$. Based on the $AICc_w$, the probability that the model fitted on $GDD5_{30}$ should be preferred to the others was 25.3%, followed by T_{min7} (22.3%), $GDD0_{21}$ (18.4%), T_{max30} (17.4%), and T_{mean21} (16.6%). The Theil's forecast accuracy coefficient did not display substantial variations among the retained models, ranging from the best scoring value of 0.417 for T_{min7} to 0.425 for T_{max30}.

The OP regressions carried out on trained models during the evaluation step fulfilled the conditions of linearity (Ramsey reset test $p > 0.05$), significance of the *F* test ($p < 0.05$) and normal distribution of the residuals (Shapiro–Wilk normality test, $p > 0.05$; Table 2). The m' and q' coefficients of the OP regressions were not significantly different from 1 and 0, respectively, with $p > 0.05$ in both cases (Table 2). Based on R^2 and RMSEP values, while the trained model with $GDD5_{30}$ as predictor scored better for its R^2 value (0.370), the minimum RMSEP was achieved by the OLS regression based on T_{max30} (0.240). All trained models were successfully validated.

3.5 | Climatic modelling of the probability associated with propagule deposition levels

The climatic analyses conducted with the adaptation of ctree models revealed that only the monthly average wind gust (MAWG) was significantly associated ($p < 0.05$) with the probability Pr(HDR) that the DR of *G. castaneae* fell in the high level range of 512–1127 spores $\cdot m^{-2} \cdot h^{-1}$ with a confidence of 95%. The ctree showed that when MAWG exceeded the threshold of 6.18 m/s (approximately 22.5 km/h), Pr(HDR) raised significantly ($p < 0.05$) from 14.3% (2.6–42.3% $CI_{95\%}$) to 100% (71.7–100% $CI_{95\%}$). The BLR model (Figure 4) met all the conditions required for its acceptability, with $\beta = 2.183$ ($p < 0.05$) and $\beta_0 = -13.141$ ($p < 0.05$), significant likelihood ratio test ($p < 0.05$), AICc = 16.2 and AICcw = 1, EPV = 12 and consequently EPV > 10, AUC = 0.95 (0.88–1.00 $CI_{95\%}$), and thus AUC > 0.5 ($p < 0.05$). The $\beta > 0$ coefficient of the model indicates a positive and significant ($p < 0.05$) correlation between the monthly average wind gust and the probability of detecting high DR levels of *G. castaneae*.

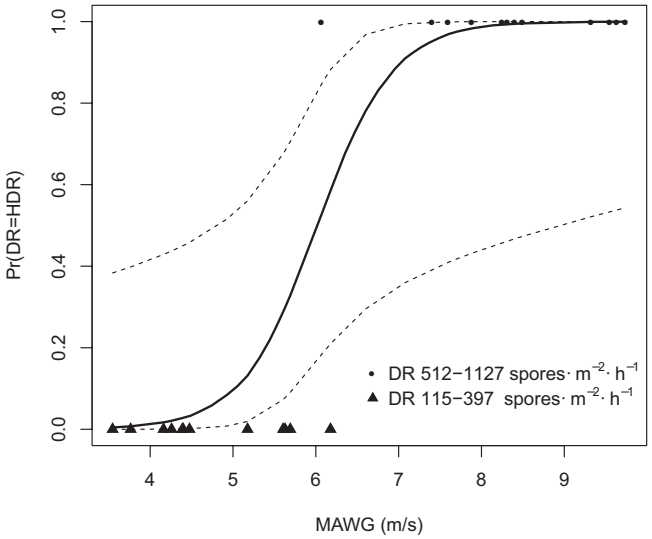

FIGURE 4 Binary logistic regression modelling the probability of observing high propagule deposition levels of *Gnomoniopsis castaneae*. Based on the monthly average wind gust (MAWG, m/s in the *x* axis), the curve predicts the probability (Pr) that the deposition rate (DR) attains a high DR level (HDR), falling in the range 512–1127 spores $\cdot m^{-2} \cdot h^{-1}$ with a confidence of 95% (on the *y* axis). Dashed lines indicate the boundaries of the 95% confidence interval of the regression. Points represent the raw data in binary form depending on the range observed in the two study sites for the DR of *G. castaneae* and on the corresponding MAWG

3.6 | Spatial distribution of propagule deposition

The Bartels test indicated a nonrandom spatial distribution of average DR along the linear transects in TS1 and TS2 ($p < 0.05$), but not in ES ($p > 0.05$). The Moran's *I* index attained a value of 0.471 ($p < 0.05$) in TS1, 0.456 ($p < 0.05$) in TS2, and −0.233 ($p > 0.05$) in ES, indicating that in TS sites spore traps were surrounded by other spore traps displaying similar values of the DR, while the spatial distribution of the DR in ES was random. This result was confirmed by the outcomes of ctree, showing that two significant clusters ($p < 0.05$) of spatially consecutive spore traps could be identified in TS1 and TS2, while in ES the DR averages were homogeneous along the transect, and hence no clusters were identified ($p > 0.05$; Figure 5). The spatial analysis conducted on a seasonal basis resulted in an inconsistent pattern of clustering of DR among sites (Table S6). However, the clustering of DR prevailed in most of the seasons both in TS1 and TS2 (Table S6).

4 | DISCUSSION

In the last decade, *G. castaneae* has been widely investigated, yet little information is available about its sporulation potential and propagule deposition patterns (Lione et al., 2019; Shuttleworth & Guest, 2017). For this reason, our goal was to carry out a long-term assessment of the propagule deposition patterns of this emerging plant pathogen. To achieve this, we developed a taxon-specific qPCR assay for *G. castaneae* that was used in combination with passive spore trapping. The spore trap devices we used were essentially based on filter paper wetted with a buffer solution that hampered propagule germination and preserved the genomic DNA; the reliability of this method has already been proved in similar aerobiological studies (Garbelotto et al., 2008). It is worth noting that the inhibition of propagule germination should prevent any bias due to the overestimation of propagule loads determined by extracting the genomic DNA of the target species (Grosdidier et al., 2017), thus contributing to a reliable assessment. In recent studies based on simple-sequence repeats (SSR) analysis, *G. castaneae* has been found to be present in Europe with at least two distinct subpopulations (Sillo et al., 2017). The subpopulations of the pathogen present in two of our study sites (TS1 and TS2) are currently known, with one subpopulation present in TS1, and the other in TS2 (Sillo et al., 2017). Consequently, our samples may be representative of both subpopulations, and hence of the whole species. It should be noted that the qPCR assay was developed and validated on isolates of both subpopulations of *G. castaneae*.

The qPCR assay and the melt curve analysis allowed *G. castaneae* to be discriminated from nontarget species, yet HRM analysis or gel electrophoresis of the qPCR products were required to discriminate *G. castaneae* from the closest related European fungal species *G. idaeicola*. No other *Gnomoniopsis* species were detected in the study sites and analysis of the subset of 19 DNA samples extracted from the spore traps demonstrated that DNA of *G. idaeicola* was absent. In addition, with the exception of *G. castaneae* on chestnut and *G. idaeicola* on *Rubus* spp., all *Gnomoniopsis* species reported in Europe so far are associated with hosts such as *Agrimonia eupatoria*, *Comarum palustre*, *Fagaria* spp., *Potentilla* spp., and *Sanguisorba minor*, which are either absent, or present with negligible abundance in chestnut stands of north-western Italy (Camerano et al., 2004; Walker et al., 2010). Therefore, all lines of evidence indicate that qPCR data obtained in this study describe the seasonal propagule deposition patterns of *G. castaneae*. Nonetheless, caution should be taken in the application of the qPCR assay in other geographical regions because of the possible presence of other *Gnomoniopsis* species not tested in this study.

Results obtained from the analytical specificity and sensitivity assays confirmed the primers' adequacy and reliability. In fact, the LOD and LOQ of the newly developed qPCR assay were appraised in different substrates to identify any differences caused by the presence of nontarget DNA or, possibly, of PCR inhibitors in environmental samples. Although both LOD and LOQ were higher in the environmental substrate than in water, they were still sufficient for the detection and quantification of *G. castaneae* DNA in the order of fg. In fact, LOQ calculated for the standard curve of conidia corresponded to approximately 3 spores $\cdot m^{-2} \cdot h^{-1}$ for an exposure of 21 days, which is a rather low amount. In this study, no specific tests were conducted to verify whether this assay would be suitable for detection and quantification of the inoculum of *G. castaneae* in other substrates, including plant tissues. Moreover, the qPCR assay does

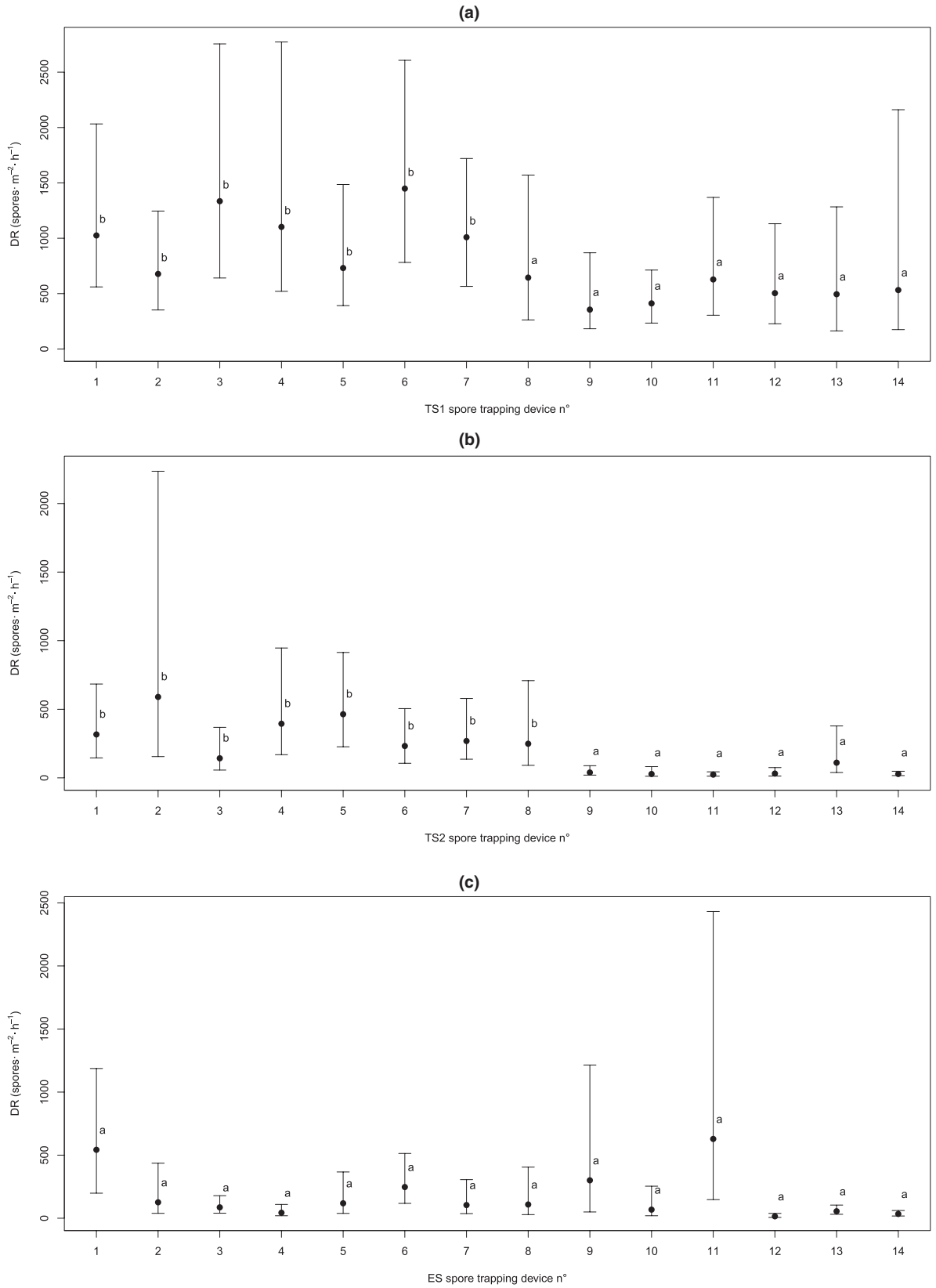

FIGURE 5 Spatial distribution of propagule deposition of *Gnomoniopsis castaneae*. The average deposition rate (DR) of *G. castaneae* (dots) and its related 95% confidence interval (whiskers) is shown for each spore trap device. Spore trap devices are labelled with progressive numbers based on their location along the linear transect. Different letters indicate the inclusion of the average DR in two significantly distinct spatial clusters ($p < 0.05$), while spore trap devices belonging to the same cluster ($p > 0.05$) are labelled with the same letter. Results are presented separately for each site: TS1 (a), TS2 (b), and ES (c)

not allow discrimination between loads of ascospores and conidia. However, this is an issue of minor concern in the case of *G. castaneae* because both ascospores and conidia are infectious and air-dispersed (Shuttleworth & Guest, 2017; Visentin et al., 2012).

The number and periodicity of samplings, as well as their geographic range were deemed adequate to achieve the desired sampling size, temporal and spatial representativeness. In fact, a total of 94 samplings were carried out during a 2-year-long timeframe at three sites located 15, 89, and 94 km apart from one another. This resulted in 1316 passive spore traps that were processed with the designed qPCR assay. It should be noted that the availability of replicates within the site (i.e., a transect of 14 traps) was pivotal for appraisal of the spatial variability and the overall uncertainty (i.e., confidence intervals) of the propagule load estimates at the site level. Temporal propagule deposition patterns of *G. castaneae* displayed a high variability among the three study sites, as indicated by the confidence intervals of the deposition rates DR and SDR, as well as by the high value achieved by the fractal dimension of their time series. Therefore, the variability of temporal propagule deposition patterns of *G. castaneae* was analysed by targeting (a) an overall variability associated with the site effect, and (b) a within-site variability associated with propagule deposition patterns free from the site effect. Different factors might be associated with the variability of the sporulation and subsequent propagule deposition levels of a plant pathogen detected with an aerobiological assay. Such factors may include, but are not limited to, the biological clock of the microorganism and its abundance, seasonal effects, climatic and environmental variables, the management practices implemented within and around the study sites, and the method used to process spore trap devices (Hospodsky et al., 2010; Kendrick, 2017). In this study, we selected seasonality and climatic factors to attempt to explain and model at least part of the variability observed in the propagule deposition patterns of *G. castaneae*. Propagules of the pathogen occur year-round, with a remarkable drop in wintertime. Inoculum sources are harboured in chestnut burrs, on *D. kuriphilus* galls and on cankers, yet other natural substrates that allow sexual/asexual reproduction of *G. castaneae* cannot be excluded due to the ecological versatility of this microorganism, which can adapt to different host plants (Lione et al., 2019; Pasche et al., 2016; Visentin et al., 2012). Thus, it is possible that infectious propagules of *G. castaneae* may be released from different inoculum sources in different periods of the year, although our experiment was not designed to investigate this.

The evidence gathered from the adaptation of ctrees to the DR and SDR of *G. castaneae* revealed that temperatures, growing degrees days, and increasing wind gust were positively correlated with higher propagule deposition levels of the pathogen; in addition, the ctrees enabled the assessment of thresholds determining a steep rise in propagule deposition. However, the effects of thermal variables and wind gust on propagule deposition patterns of *G. castaneae* were different, thermal variables being associated with the fluctuations of propagule deposition within sites while wind gust related to the propagule abundance at the site level.

Warming temperatures and increasing growing degree days were positively correlated with SDR of *G. castaneae* and explained 35.8%–82.2% of the variability. OLS regressions performed satisfactorily in the training and evaluation steps of the machine learning process. By combining the results of both steps, the best scoring model of the temporal propagule deposition patterns of *G. castaneae* was that based on the growing degree days with threshold 5°C. This result seems to corroborate the conclusions drawn by Lovell et al. (2004), who proposed the replacement of physical time with thermal related units of measurement, such as growing degree days. In fact, lines of evidence from different case studies suggested that thermal time could be more appropriate for investigation of temporal patterns associated with the epidemiology of plant pathogens (Lovell et al., 2004). Importantly, the growing degree days are not only associated with propagule deposition patterns of *G. castaneae*, as demonstrated in this study, but they are also acknowledged as strongly correlated with the phenology of host plants, including flowering (Lovell et al., 2004). Moreover, the base temperature of 5°C used for the calculation of the growing degree days is consistent with the threshold reported in other studies investigating climatology and plant–microbe interactions (Puentes et al., 2007; Ruosteenoja et al., 2016), and matches the lower boundary of the cardinal temperatures assessed by Visentin et al. (2012) for *G. castaneae* (i.e., 5°C). In addition, the prominent role of temperatures in driving the propagule deposition of *G. castaneae* is consistent with previous results showing that increasing minimum, maximum, and average temperatures are positively and significantly correlated with nut rot incidence at harvesting (Lione et al., 2015). The climatic data collection was conducted either with in-site equipment, or according to the methods previously employed to investigate the association between climatic variables and the incidence of G. *castaneae* at the site level (Lione et al., 2015). Hence, the analysis of climatic data through machine learning is supported by a robust experimental design. However, this design was not conceived to account for microclimatic factors that might exert effects at the scale of a few metres, but to unravel the association between climatic variables and the propagule deposition patterns of *G. castaneae* at the site level.

To date, the floral route is the only infection pathway documented for this pathogen, which supports the hypothesis that infections of *G. castaneae* leading to nut rots are fostered by warmer temperatures at flowering time. However, other natural or anthropic-mediated infection pathways through stomata, infected seeds, or wounds cannot be excluded. Also, insects might play a role as vectors of infectious inoculum of *G. castaneae* (Shuttleworth & Guest, 2017), although this hypothesis is still not supported by experimental evidence (Lione et al., 2019). Recently, results from a study investigating the association between the Asian gall wasp *D. kuriphilus* and *G. castaneae* excluded the possibility that this insect may be a vector of viable inoculum of the fungus (Lione et al., 2016). Although several other species of insect were observed in association with chestnut in our study sites, including *Apis mellifera*, *Bombus* spp., *Coccinella septempunctata*, *Curculio elephas*, *Cydia* spp., their role in the epidemiology of *G. casteneae* still needs to be elucidated.

Based on the disease triangle paradigm, although airborne propagules can be present during most of the year, their epidemiological role depends upon the receptivity of the susceptible host exposed to the pathogenic inoculum. Host receptivity may vary in relation to several factors, such as host phenology and management practices. While our study focused on modelling the potential exposure of the host to airborne propagules of *G. castaneae*, the investigation of host receptivity is probably one of the upcoming challenges that researchers should tackle to fill the gaps in our knowledge of the biological cycle of *G. castaneae*. Management practices in the orchards of our study are unlikely to have produced substantial effects on our results. In fact, all study sites were traditional chestnut orchards characterizing the typical landscape of hills and mountain areas across north-western Italy, southern France, and Switzerland (Gullino et al., 2020; Lione et al., 2015). Sampled orchards were mature chestnut stands, traditionally managed by local owners, who restricted operations to grass cutting and harvesting of nuts by hand (Gullino et al., 2020). Significantly, no anomalous peaks in the propagule deposition were observed after such operations were carried out and, during our 2-year long experiment, no other operations affecting the trees, the litter or the soil (e.g., pruning, thinning, chipping, excavation) were conducted. Because the management of orchards was minimal and similar across the three sampling sites, our experimental design was not suitable for assessing or comparing the effects of management practices on the propagule deposition pattern of *G. castaneae*. In addition, tree density was comparable among the study sites, even though variations in tree density are unlikely to substantially influence the propagule deposition rates of the fungus, as previously noted (Lione & Gonthier, 2016). Specific studies are needed to shed light on the potential effects of management practices on the sporulation potential and incidence of *G. castaneae*.

Neither relative humidity nor precipitations were significantly associated with propagule deposition of *G. castaneae*. In a previous modelling effort carried out in Europe, we failed to detect any significant association between disease incidence and rainfall during the flowering period (Lione et al., 2015); this is fully consistent with the findings presented in the present paper. It should be noted that the effects of precipitation on the infection process may also depend on their intensity (Kendrick, 2017). While mild and short rainfalls are reported to boost the discharge of spore loads, heavy or prolonged precipitation may have an opposite effect (Kendrick, 2017). Nonetheless, we included as potential predictors for the temporal propagule deposition patterns of *G. castaneae* the number of days characterized by different thresholds of precipitation, from 0 to 30 mm/day, to account for both mild and heavy rainfall events.

We cannot exclude the possibility that the differences in propagule deposition levels between TS1 and TS2 were linked to the overall abundance of the fungus at the two sites and/or to the two different subpopulations of the pathogen mentioned above, which might differ in some phenotypic traits, including sporulation ability. Specific experiments need to be conducted to test these hypotheses. While the overall disease incidence was similar at the two sites, suggesting that the pathogen could be present with comparable abundance, in this study we showed that wind gust was the only significant climatic driver, explaining the 4:1 ratio of propagule deposition level of *G. castaneae* between TS1 and TS2. Based on our results, when the average monthly wing gust exceeds the value of 6.18 m/s, the overall DR is likely to jump from roughly 100–400 to 500–1000 spores $\cdot m^{-2} \cdot h^{-1}$. The outcomes of the binary logistic regression model were consistent, showing that the probability of observing a high overall average deposition level of *G. castaneae* raised with increasing average monthly wind gusts. These lines of evidence suggest that wind may affect, at the site-scale, the overall baseline around which temperatures determine the fluctuations of the spore loads of *G. castaneae*. This interpretation is consistent with the role of increasing wind gust in fostering the release of spores of plant pathogens, as well as their spread (Viljanen-Rollinson et al., 2007).

In two out of three sites, DR was clustered in hotspots of low or high values, which might indicate that the deposition of spores, and possibly their release, increases in proximity to high concentrations of inoculum sources (e.g., accumulation of burrs on the litter). This finding suggests a limited dispersal range of *G. castaneae* propagules, and hence the potential efficacy of all agronomic measures that result in the removal or inactivation of inoculum sources from the site, as previously hypothesized (Sillo et al., 2017). Based on this finding, we may also speculate that wind gusts may be more effective in the liberation rather than in the dispersal of propagules of *G. castaneae*.

In conclusion, temporal patterns of propagule deposition of *G. castaneae* have been determined in some orchards of north-western Italy by combining passive spore trapping with a newly developed taxon-specific qPCR assay. These patterns proved to be consistent among sites and driven by temperatures. Wind gust has been identified as a climatic factor associated with the number of propagules deposited at site level. In perspective, the increase in temperatures and strong winds as a result of climate change might boost infections by *G. castaneae* and increase its impact on chestnut and other susceptible hosts.

ACKNOWLEDGEMENTS

This research was funded by Regione Piemonte through the F.E.A.S.R. 2014/2020, Projects #castagnopiemonte and 3C (Progetti pilota per la Cooperazione ed il miglioramento della Competitività della Castanicoltura regionale) and through the activity of the Chestnut R&D Center; by the European Commission through the programme INTERREG V-A Italy-Switzerland 2014/2020, Project MONGEFITOFOR id 540693 (linee guida per il MOnitoraggio e la Gestione delle Emergenze FITOsanitarie nelle FOReste delle Alpi centro-occidentali); and by the University of Torino in the framework of 60% Projects. The authors wish to thank the owners of chestnut orchards in San Giorio di Susa, Peveragno, and Gaiola for the in-field support, and Riccardo Dipoppa for the laboratory assistance in the processing of spore traps. The authors wish to thank the editors and the reviewers for their useful comments enabling the improvement of the quality of the manuscript. The authors have no conflicts of interest to declare.

DATA AVAILABILITY STATEMENT

All data relevant to this manuscript are provided as supplementary files.

ORCID

Guglielmo Lione https://orcid.org/0000-0002-3777-0813
Luana Giordano https://orcid.org/0000-0003-1686-6338
Fabiano Sillo https://orcid.org/0000-0002-1218-9985
Francesca Brescia https://orcid.org/0000-0002-2135-1286
Paolo Gonthier https://orcid.org/0000-0002-7242-8239

REFERENCES

ARPA Piemonte. (2020) *Banca Dati Meteorologica e Idrologica*. http://www.arpa.piemonte.it. [Accessed 27 October 2019].

Camerano, P., Gottero, F., Terzuolo, P. & Varese, P. (2004) *I Tipi Forestali del Piemonte*, Italy: Regione Piemonte – Blu Edizioni.

Crawley, M.J. (2013) *The R Book*, 2nd edition. Chichester, U.K.: John Wiley & Sons.

Desimoni, E. & Brunetti, B. (2015) About estimating the limit of detection by the signal to noise approach. *Pharmaceutica Analytica Acta*, *6*, 1–4.

Fick, S.E. & Hijmans, R.J. (2017) WorldClim 2: new 1-km spatial resolution climate surfaces for global land areas. *International Journal of Climatology*, *37*, 4302–4315.

Ganthaler, A. & Mayr, S. (2015) Temporal variation in airborne spore concentration of *Chrysomyxa rhododendri*: correlation with weather conditions and consequences for Norway spruce infection. *Forest Pathology*, *45*, 443–449.

Garbelotto, M., Schmidt, D., Swain, S., Hayden, K. & Lione, G. (2017) The ecology of infection between a transmissive and a dead-end host provides clues for the treatment of a plant disease. *Ecosphere*, *8*, e01815.

Garbelotto, M., Smith, T. & Schweigkofler, W. (2008) Variation in rates of spore deposition of *Fusarium circinatum*, the causal agent of pine pitch canker, over a 12-month-period at two locations in northern California. *Phytopathology*, *98*, 137–143.

Gneiting, T., Ševčíková, H. & Percival, D.B. (2012) Estimators of fractal dimension: assessing the roughness of time series and spatial data. *Statistical Science*, *27*, 247–277.

Gonthier, P., Garbelotto, M. & Nicolotti, G. (2005) Seasonal patterns of spore deposition of *Heterobasidion* species in four forests of the western Alps. *Phytopathology*, *95*, 759–767.

Grosdidier, M., Aguayo, J., Marçais, B. & Ioos, R. (2017) Detection of plant pathogens using real-time PCR: how reliable are late C_t values? *Plant Pathology*, *66*, 359–367.

Grosdidier, M., Ioos, R., Husson, C., Cael, O., Scordia, T. & Marçais, B. (2018) Tracking the invasion: dispersal of *Hymenoscyphus fraxineus* airborne inoculum at different scales. *FEMS Microbiology Ecology*, *94*, fiy049.

Gullino, P., Mellano, M.G., Beccaro, G.L., Devecchi, M. & Larcher, F. (2020) Strategies for the management of traditional chestnut landscapes in Pesio Valley, Italy: a participatory approach. *Land*, *9*, 536.

Hasnain, S.M. (1993) Influence of meteorological factors on the airspora. *Grana*, *32*, 184–188.

Hospodsky, D., Yamamoto, N. & Peccia, J. (2010) Accuracy, precision, and method detection limits of quantitative PCR for airborne bacteria and fungi. *Applied and Environmental Microbiology*, *76*, 7004–7012.

Hothorn, T., Hornik, K. & Zeileis, A. (2006) Unbiased recursive partitioning: a conditional inference framework. *Journal of Computational and Graphical Statistics*, *15*, 651–674.

Jackson, S.L. & Bayliss, K.L. (2011) Spore traps need improvement to fulfil plant biosecurity requirements. *Plant Pathology*, *60*, 801–810.

Jiang, N. & Tian, C. (2019) An emerging pathogen from rotted chestnut in China: *Gnomoniopsis daii* sp. nov. *Forests*, *10*, 1016.

Kendrick, B. (2017) *The Fifth Kingdom. An Introduction to Mycology*, 4th edition. Cambridge, MA: Hackett Publishing.

Kowalski, T. (2006) *Chalara fraxinea* sp. nov. associated with dieback of ash (*Fraxinus excelsior*) in Poland. *Forest Pathology*, *36*, 264–270.

Lantz, B. (2019) *Machine learning with R: Expert techniques for predictive modeling*. Birmingham, U.K.: Packt Publishing Ltd.

Lione, G., Danti, R., Fernandez-Conradi, P., Ferreira-Cardoso, J.V., Lefort, F., Marques, G. et al (2019) The emerging pathogen of chestnut *Gnomoniopsis castaneae*: the challenge posed by a versatile fungus. *European Journal of Plant Pathology*, *153*, 671–685.

Lione, G., Giordano, L., Ferracini, C., Alma, A. & Gonthier P. (2016) Testing ecological interactions between *Gnomoniopsis castaneae* and *Dryocosmus kuriphilus*. *Acta Oecologica*, *77*, 10–17.

Lione, G., Giordano, L., Sillo, F. & Gonthier, P. (2015) Testing and modelling the effects of climate on the incidence of the emergent nut rot agent of chestnut *Gnomoniopsis castanea*. *Plant Pathology*, *64*, 852–863.

Lione, G., Giordano, L., Turina, M. & Gonthier, P. (2020) Hail-induced infections of the chestnut blight pathogen *Cryphonectria parasitica* depend on wound size and may lead to severe diebacks. *Phytopathology*, *110*, 1280–1293.

Lione, G. & Gonthier, P. (2016) A permutation-randomization approach to test the spatial distribution of plant diseases. *Phytopathology*, *106*, 19–28.

Lovell, D.J., Powers, S.J., Welham, S.J. & Parker, S.R. (2004) A perspective on the measurement of time in plant disease epidemiology. *Plant Pathology*, *53*, 705–712.

Pasche, S., Calmin, G., Auderset, G., Crovadore, J., Pelleteret, P., Mauch-Mani, B. et al (2016) *Gnomoniopsis smithogilvyi* causes chestnut canker symptoms in *Castanea sativa* shoots in Switzerland. *Fungal Genetics and Biology*, *87*, 9–21.

Petäistö, R.L. & Heinonen, J. (2003) Conidial dispersal of *Gremmeniella abietina*: climatic and microclimatic factors. *Forest Pathology*, *33*, 363–373.

Piñeiro, G., Perelman, S., Guerschman, J.P. & Paruelo, J.M. (2008) How to evaluate models: observed vs. predicted or predicted vs. observed? *Ecological Modelling*, *216*, 316–322.

Puentes, A., Bazely, D.R. & Huss-Danell, K. (2007) Endophytic fungi in *Festuca pratensis* grown in Swedish agricultural grasslands with different managements. *Symbiosis*, *44*, 121–126.

Regione Piemonte - DB0800 - Programmazione strategica, Politiche territoriali ed Edilizia - DB0816 - Cartografia e Sistema Informativo Territoriale. (2009) *Modelli digitali del terreno da CTR 1:10.000*. https://www.geoportale.piemonte.it/cms/ [Accessed 20 June 2021].

Regione Piemonte - A1613B - Sistema informativo territoriale e ambientale. (2005) *CTR (Carta Tecnica Regionale) raster 1:10.000 (1991-1995)*. https://www.geoportale.piemonte.it/cms/ [Accessed 20 June 2021].

Ruosteenoja, K., Räisänen, J., Venäläinen, A. & Kämäräinen, M. (2016) Projections for the duration and degree days of the thermal growing season in Europe derived from CMIP5 model output. *International Journal of Climatology*, *36*, 3039–3055.

Shuttleworth, L.A. & Guest, D.I. (2017) The infection process of chestnut rot, an important disease caused by *Gnomoniopsis smithogilvyi* (*Gnomoniaceae*, *Diaporthales*) in Oceania and Europe. *Australasian Plant Pathology*, *46*, 397–405.

Shuttleworth, L.A., Guest, D.I. & Liew, E.C.Y. (2012) Fungal planet description sheet 108: *Gnomoniopsis smithogilvyi* L.A. Shuttleworth, E.C.Y. Liew & D.I. Guest, sp. nov. *Persoonia*, *28*, 142–143.

Sillo, F., Giordano, L., Zampieri, E., Lione, G., De Cesare, S. & Gonthier, P. (2017) HRM analysis provides insights on the reproduction mode and the population structure of *Gnomoniopsis castaneae* in Europe. *Plant Pathology*, *66*, 293–303.

Skjøth, C.A., Damialis, A., Belmonte, J., De Linares, C., Fernández-Rodríguez, S., Grinn-Gofroń, A. et al (2016) *Alternaria* spores in the air across Europe: abundance, seasonality and relationships with climate, meteorology and local environment. *Aerobiologia*, *32*, 3–22.

Thomas, J.E., Wood, T.A., Gullino, M.L. & Ortu, G. (2017) Diagnostic tools for plant biosecurity. In: Gullino, M.L., Stack, J., Fletcher, J. & Mumford, J. (Eds.) *Practical tools for plant and food biosecurity. Plant pathology in the 21st century*. Cham, Switzerland: Springer, pp. 209–226.

Van Maanen, A. & Xu, X.M. (2003) Modelling plant disease epidemics. *European Journal of Plant Pathology*, *109*, 669–682.

Viljanen-Rollinson, S.L.H., Parr, E.L. & Marroni, M.V. (2007) Monitoring long distance spore dispersal by wind a review. *New Zealand Plant Protection*, *60*, 291–296.

Visentin, I., Gentile, S., Valentino, D., Gonthier, P., Tamietti, G. & Cardinale, F. (2012) *Gnomoniopsis castanea* sp. nov. (Gnomoniaceae, Diaporthales) as the causal agent of nut rot in sweet chestnut. *Journal of Plant Pathology*, *94*, 411–419.

Walker, D.M., Castlebury, L.A., Rossman, A.Y., Sogonov, M.V. & White, J.F. (2010) Systematics of genus *Gnomoniopsis* (Gnomoniaceae, Diaporthales) based on a three gene phylogeny, host associations and morphology. *Mycologia*, *102*, 1479–1496.

West, J.S. & Kimber, R.B.E. (2015) Innovations in air sampling to detect plant pathogens. *Annals of Applied Biology*, *166*, 4–17.

White, T.J., Bruns, T., Lee, S. & Taylor, J. (1990) Amplification and direct sequencing of fungal ribosomal RNA genes for phylogenetics. In: Innis, M.A., Gelfand, D.H. & Sninsky, J.J. (Eds.) *PCR protocols. A guide to methods and applications*. San Diego, CA: Academic Press, pp. 315–322.

Wickham, H. (2010) A layered grammar of graphics. *Journal of Computational and Graphical Statistics*, *19*, 3–28.

Willocquet, L. & Clerjeau, M. (1998) An analysis of the effects of environmental factors on conidial dispersal of *Uncinula necator* (grape powdery mildew) in vineyards. *Plant Pathology*, *47*, 227–233.

Wyka, S.A., McIntire, C.D., Smith, C., Munck, I.A., Rock, B.N., Asbjornsen, H. et al (2018) Effect of climatic variables on abundance and dispersal of *Lecanosticta acicola* spores and their impact on defoliation on eastern white pine. *Phytopathology*, *108*, 374–383.

SUPPORTING INFORMATION

Additional supporting information may be found online in the Supporting Information section.

How to cite this article: Lione, G., Giordano, L., Sillo, F., Brescia, F. & Gonthier, P. (2021) Temporal and spatial propagule deposition patterns of the emerging fungal pathogen of chestnut *Gnomoniopsis castaneae* in orchards of north-western Italy. *Plant Pathology*, 70, 2016–2033. https://doi.org/10.1111/ppa.13451